mathematics

MDPI

Article

Applications of Discrete Wavelet Transform for Feature Extraction to Increase the Accuracy of Monitoring Systems of Liquid Petroleum Products

Mohammed Balubaid [1], Mohammad Amir Sattari [2], Osman Taylan [1], Ahmed A. Bakhsh [1] and Ehsan Nazemi [3,*]

[1] Department of Industrial Engineering, Faculty of Engineering, King Abdulaziz University, P.O. Box 80204, Jeddah 21589, Saudi Arabia; mbalubaid@kau.edu.sa (M.B.); otaylan@kau.edu.sa (O.T.); aabakhsh@kau.edu.sa (A.A.B.)
[2] Friedrich Schiller University Jena, Fürstengraben 1, 07743 Jena, Germany; mohamadamir.sattari@gmail.com
[3] Imec-Vision Lab, Department of Physics, University of Antwerp, 2610 Antwerp, Belgium
* Correspondence: ehsan.nazemi@uantwerpen.be

Abstract: This paper presents a methodology to monitor the liquid petroleum products which pass through transmission pipes. A simulation setup consisting of an X-ray tube, a detector, and a pipe was established using a Monte Carlo n-particle X-version transport code to investigate a two-by-two mixture of four different petroleum products, namely, ethylene glycol, crude oil, gasoline, and gasoil, in deferent volumetric ratios. After collecting the signals of each simulation, discrete wavelet transform (DWT) was applied as the feature extraction system. Then, the statistical feature, named the standard deviation, was calculated from the approximation of the fifth level, and the details of the second to fifth level provide appropriate inputs for neural network training. Three multilayer perceptron neural networks were utilized to predict the volume ratio of three types of petroleum products, and the volume ratio of the fourth product could easily be obtained from the results of the three presented networks. Finally, a root mean square error of less than 1.77 was obtained in predicting the volume ratio, which was much more accurate than in previous research. This high accuracy was due to the use of DWT for feature extraction.

Keywords: wavelet transform; feature extracting; monitoring system; petroleum products

Citation: Balubaid, M.; Sattari, M.A.; Taylan, O.; Bakhsh, A.A.; Nazemi, E. Applications of Discrete Wavelet Transform for Feature Extraction to Increase the Accuracy of Monitoring Systems of Liquid Petroleum Products. *Mathematics* **2021**, *9*, 3215. https://doi.org/10.3390/math9243215

Academic Editors: Frank Werner and Ezequiel Lopez Rubio

Received: 19 October 2021
Accepted: 10 December 2021
Published: 13 December 2021

1. Introduction

In the petrochemical industry, poly-pipelines are commonly used to transport oil or its derivatives to distribution centers. Using one pipeline to transport different petroleum fluids is very cost-effective, but the existence of problems, such as combinations of various petroleum fluids, shows the importance of developing a non-invasive method in controlling and detecting the interference region. For this reason, many types of research have been conducted, which are briefly reviewed. Salgado et al. developed a petrochemical product density detection system that included a Cs-137 source and a sodium iodide (NaI) detector [1]. The Monte Carlo N-Particle X-version (MCNPX) transport code was used in this study. Using an artificial neural network enabled prediction of the density of petroleum products with high accuracy, independent of fluid composition. They also performed a laboratory experiment to validate the Monte Carlo code, using a cesium source, a glass pipe, and a sodium iodide detector. Different volume percentages were simulated for both oil and water fluids. The volume percentages could be detected with an accuracy of 1% [2]. In other studies, researchers simulated two-phase [3–5] and three-phase [6–8] compositions at different volumetric percentages and different flow regimes. Various neural networks with different training algorithms, such as MLP [9,10], RBF [11,12], adaptive neuro-fuzzy inference systems [13], Jaya algorithms [14], and GMDH neural networks [15] were applied

to predict volume percentages and flow regimes with high accuracy. In recent years, the use of feature extraction techniques such as time domain [16,17], frequency domain [18], and time–frequency domain [19] has been widely considered by researchers in this field. In all the above mentioned studies, the researchers presented different characteristics for distinguishing the type of flow regimes and determining the volume percentages. Sattari et al. used GMDH neural networks to recognize the type of flow regimes [20]. They simulated a structure including a Cs-137 radioisotope, a Pyrex pipe, and a NaI detector using the MCNPX transport code. They extracted the time domain characteristics of the recorded signal and considered them as neural network inputs. Estimation of volume percentages with a RMSE of less than 1.11 was the result of this investigation.

Recently, the use of X-ray tubes has been very popular with researchers because of their many benefits. The use of X-ray tubes as a source has the following advantages compared to other sources such as radioisotopes: X-ray tubes can adjust the emitted photon energy, whereas the photon emission energy is constant in radioisotopes. It should also be noted that the activity of radioisotopes decreases over time, but X-ray tubes do not follow this rule; X-ray tubes can be turned on and off. They are also easier to transport than radioisotopes. In their recent study, Roshani et al. proposed a system for monitoring fluids passing through transfer tubes [21]. Although they were able to predict the volumetric ratio of petroleum products with a MAE of less than 2.72, the use of feature extraction techniques can increase the accuracy of such systems. Much research has been conducted to measure the volume fractions of two-phase [22,23] and three-phase [24,25] flows using X-ray tubes. Researchers have claimed that the feature extraction techniques can help increase the accuracy of determining the type of flow regimes. In their study, Hosseini et al. [26] simulated a laboratory structure with an MCNP transport code in which they implemented three homogeneous, stratified, and annular regimes in different volume percentages. A cesium-137 source and a NaI detector were used in this simulation. Using the wavelet feature extraction technique combined with a neural network, they succeeded to fully recognize flow regimes and estimate volume percentages with an acceptable accuracy. In another study, Henus and colleagues implemented four flow regimes in a horizontal pipe named slug, bubble, and transitional plug–bubble flows to determine the type of flow regimes using a gamma ray absorption technique and wavelet feature extraction [27]. Further studies [28,29] have explored the applications of wavelet feature extraction in the field of radiation absorption signals.

Inspired by previous research, in this study, an attempt has been made to propose a high-precision monitoring system that can determine the volume ratio of different oil products. This article is organized as follows: first, the structure of the simulation will be explained in detail; the next section presents the discrete wavelet transform (DWT) method for extracting the received signal characteristics; in the third section, multilayer perceptron (MLP) neural networks will be discussed, and the results and accuracy of the designed networks will be shown; the last section concludes the study.

2. Simulation System

The simulation setup consisted of an X-ray tube, a pipe, and a NaI detector (Figure 1), and was performed using MCNPX [30]. A simulation of a typical industrial X-ray tube was used in this study. The real X-ray source consisted of an electron source and a tungsten target, which were mounted in an X-ray tube shield [31,32]. With the aim of reducing the simulation calculation time, a photon source inserted in the shield was regarded as a cathode–anode assembly in this investigation. The spectrum obtained from the TASMIC package [33] was also implemented to model the photon source energy. Figure 2 shows the normalized X-ray spectrum, as well as the features of X-ray peaks related to the tungsten target (Kα1, Kα2, Kβ1, and Kβ2). The circular section on the X-ray tube which was considered as the output window was 5 cm. Notably, the cylindrical form frequently shaped the X-ray tube shields, which were also made of lead or steel to prevent the emission of harmful radiation produced by X-rays.

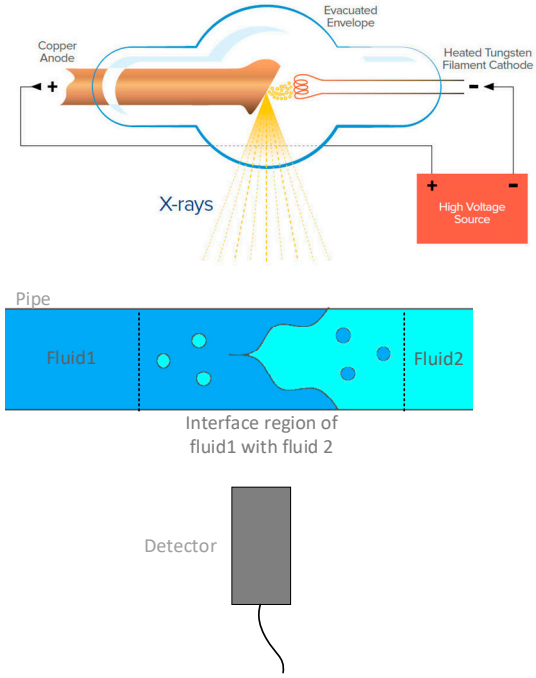

Figure 1. The simulation setup.

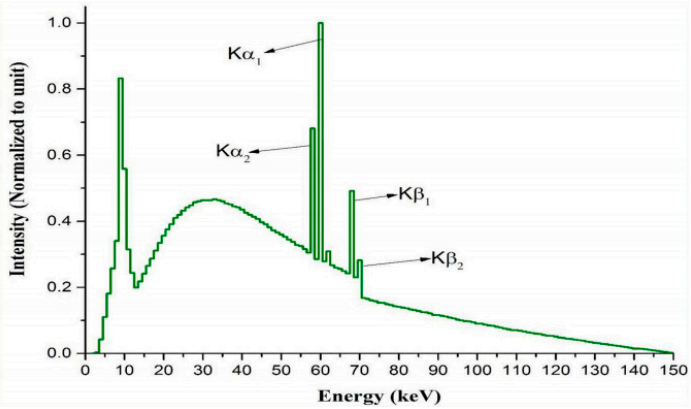

Figure 2. The X-ray spectrum derived from TASMIC package.

Transmission pipes are used to transport various petroleum products, some parts of which interact with each other and are mixed together. This area is known as the interface region. In this research, four types of petroleum products—ethylene glycol, crude oil, gasoil, and gasoline—are considered as fluids passing through the pipe. By mixing all of the listed products two-by-two, six combinations were obtained. Various volume ratios from 0% to 100%, with steps of 5%, were simulated for all six different states (in this study, 118 simulations were performed in total). Data from all simulations were collected by a simulated NaI detector and used for later processing.

3. Discrete Wavelet Transform

Discrete wavelet transform (DWT) is the most commonly used method in the filtering of time–frequency [34]. The reduction of additive noises by DWT provides good resolution in the frequency and time domains. Multi-resolution analysis is enabled by the DWT method by dividing the discrete signal x(n) into low- and high-frequency components. To determine DWT, an iterative Mallat algorithm can be applied [35,36]. The low-frequency

component $a_{j,k}$ (approximately) and the high-frequency component $d_{j,k}$ (exactly) (Figure 3) are the results of signal x(n) decomposition with multi-level filter banks:

$$a_{j,k} = \sum_{l} h(l-2k)a_{j-1,m} \tag{1}$$

$$d_{j,k} = \sum_{l} g(l-2k)a_{j-1,m} \tag{2}$$

where j is a parameter that affects the DWT scaling. k is related to the translation at each level of the wavelet function. l is the number of levels and is an integer scale. $h(l)$ and $g(l)$ are low-pass and high-pass square filters, respectively. m is utilized in the scaling function as a translation of the j scale. Daubechies, Haar, etc., are several families of wavelet functions that exist in wavelet transform. In the present study, a Daubechies 2 (db2) wavelet was selected to analyze the signals received from the scintillation detector.

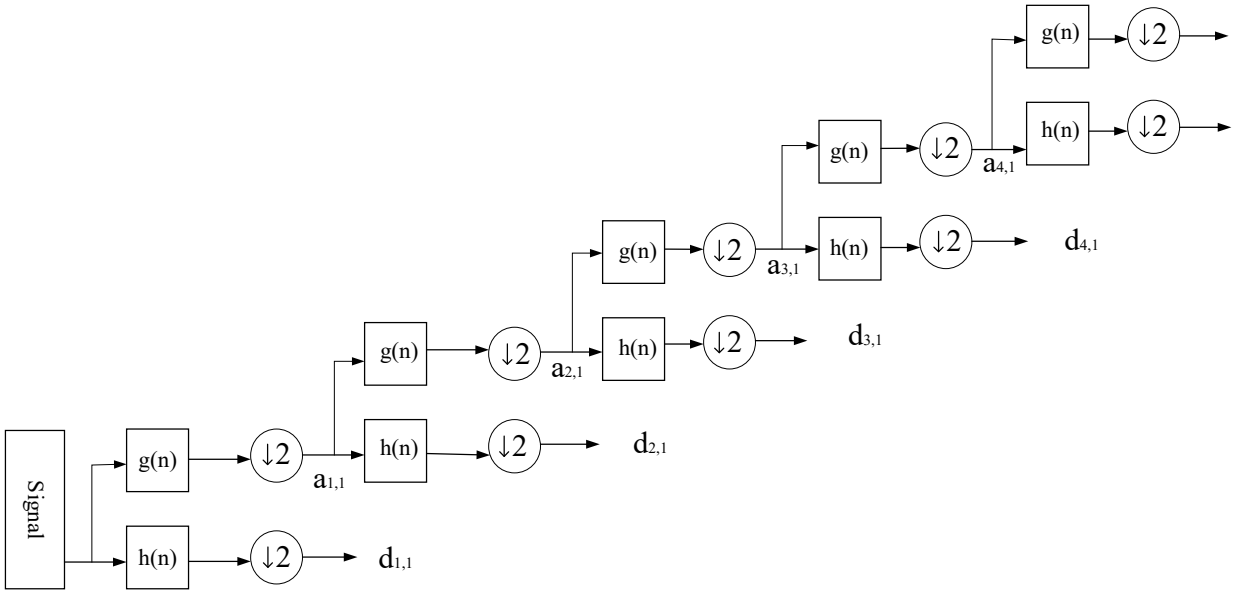

Figure 3. The signal decomposition process using DWT; g(n) is the low-pass filter, h(n) is the high-pass filter. The operator ↓2 means down-sampling by two.

The decomposition process of the signal obtained by the detector is illustrated in Figure 4. According to this figure, from the fifth stage onwards, no significant high-frequency information was obtained; thus, in this study, the signal decomposition only continued until the fifth stage. It should be noted that the details of the first stage had many fluctuations that show noisy behavior. The researchers believe that this signal is due to uncertainty problems in the MCNPX transport code. Therefore, these details were not considered for the next processing step. To provide suitable data for network inputs, the standard deviation (STD) features of $a_{5,1}$, $d_{5,1}$, $d_{4,1}$, $d_{3,1}$, and $d_{2,1}$ have been calculated. It should be noted that this statistical characteristic has been introduced in previous studies as an efficient time characteristic [16].

$$TD = \sqrt{\frac{1}{N-1}\sum_{i=1}^{N}|x_i - \mu|^2} \tag{3}$$

$$\mu = \frac{1}{N}\sum_{i=1}^{N} x_i \tag{4}$$

where x_i is the primary data and N is the amount of data.

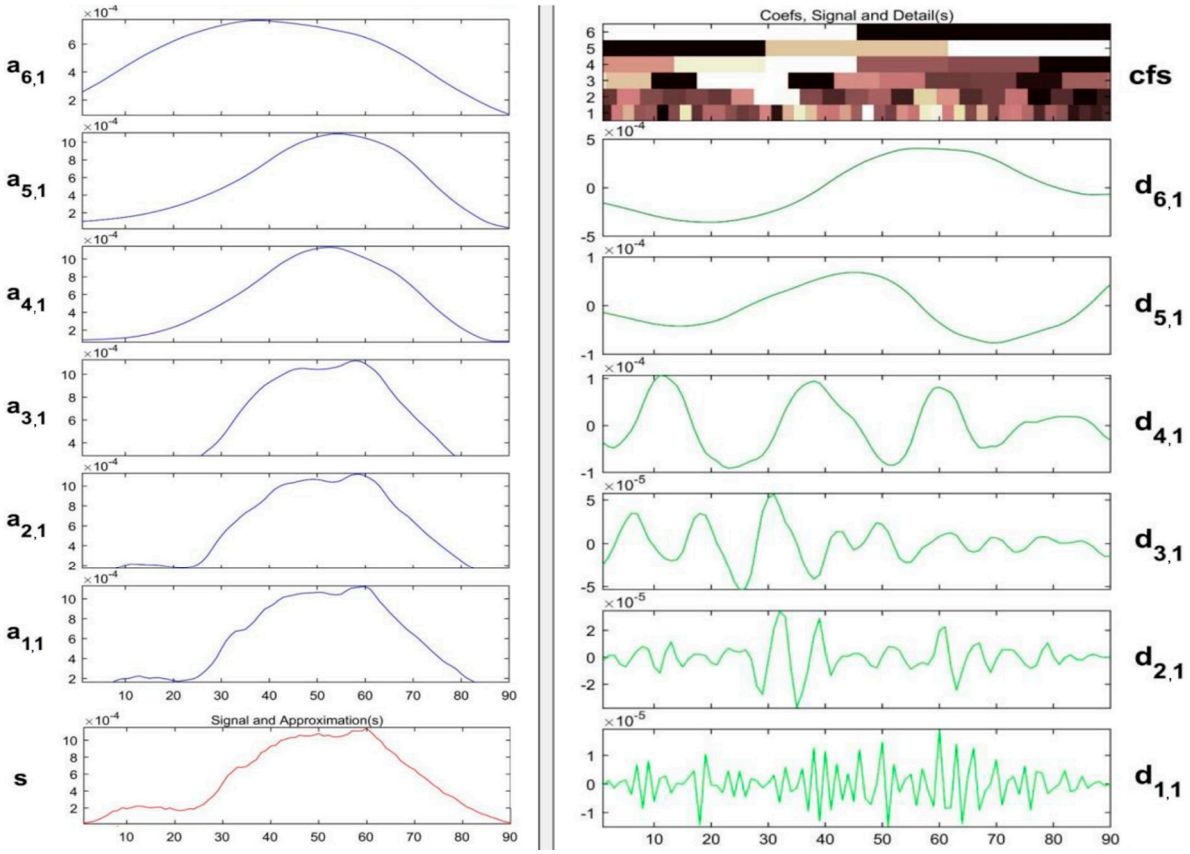

Figure 4. The results of signal decomposition into approximations and details.

4. MLP Neural Network

In recent years, various advanced computational approaches have been applied in different fields such as chemical engineering [37–44], control and electrical engineering [45–59], pharmacy and medical science [60–67], industrial engineering [68,69], civil engineering [70–73], economic and business sciences, [74–78], mechanical engineering [79–85], energy engineering [86–89], computer and information technology [90–102], physics [103–108], mining engineering [109–111], petroleum engineering [112–116], mathematics [117–124], etc. MLP neural networks are one of the most powerful tools used in predicting, classifying, modeling, and optimizing. This network has become one of the most widely used neural networks due to the various applications for which it has been developed. This network is able to perform nonlinear mapping with high accuracy, which is what was used as the main solution in various problems. This is a feedforward network where the output is calculated directly from the input without any feedback with the backpropagation (BP) algorithm. The BP algorithm means that after determining the network's output, first, the weights of the final layer are corrected, and then the weights of the previous layers are corrected respectively. The neuron model in the multilayer perceptron network includes a nonlinear activator function. The output of a perceptron in an MLP neural network is obtained based on Equation (6) [125,126]:

$$output = f\left(\sum_{i=1}^{n} x_i w_i + b\right) \tag{5}$$

In the above equation, x represents the network inputs, w depicts the network weights, b is the bias, f is the activating function of the neurons, and n represents the number of inputs.

The perceptron implementation algorithm is the first random values assigned to weights. Perceptron is then applied to all training data. If the example is evaluated incorrectly, the values of perceptron weights are corrected. The collected data are divided into three categories: training, validation, and testing data. Training data are used to estimate network weights to create a neural network model; validation data are used to test during the training process; and test data are used to evaluate the trained network. Using these data, the ability of the designed neural network in prediction is determined. In this study, 70% of the data were used for training, 15% were allocated to the validation section, and 15% were used for network testing. In this research, to find the most optimal structure, networks with one, two, three and four layers, and with different number of neurons in each layer, have been designed, and their functions have been evaluated. MATLAB R2018b software was used to train neural networks.

5. Result and Discussion

In this study, the characteristics extracted in the previous section were considered the neural network's inputs. Three neural networks were implemented to estimate the volume ratios of ethylene glycol, crude oil, and gasoil. By determining the volume ratio of the three mentioned products, the ratio of the fourth product, i.e., gasoline, could easily be calculated. Figure 5 and Table 1 show the structure of the implemented networks.

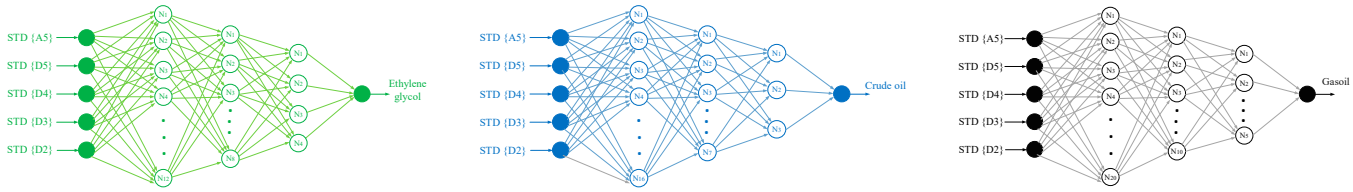

(**a**) (**b**) (**c**)

Figure 5. The structure of the implemented MLP neural network for prediction of (**a**) ethylene glycol, (**b**) crude oil, and (**c**) gasoil volumetric ratios.

Table 1. The specifications of the designed networks.

ANN Type	MLP		
	Ethylene Glycol	**Gasoil**	**Crude Oil**
No. of input layer neurons	5	5	5
No. of 1st hidden layer neurons	12	20	16
No. of 2nd hidden layer neurons	8	10	7
No. of 3rd hidden layer neurons	4	5	3
No. of output layer neurons	1	1	1
No. of epochs	650	800	550
Activation function used for each hidden neuron	Tansig	Tansig	Tansig

Regression and error diagrams related to training, validation, and test data can be seen in Figures 6–8, presenting the accuracy of the designed networks. The most important criterion for evaluating the performance of artificial neural networks is the accuracy of prediction. Some of the most important prediction accuracy criteria calculated in this study are:

$$\text{Root Mean Square Error } (RMSE) = \frac{\sum_{j=1}^{N} (e_j)^2}{N} \tag{6}$$

$$\text{Mean Absolut Error } (MAE) = \frac{1}{N} \sum_{j=1}^{N} |e_j| \tag{7}$$

where e is the error, y is the network output, and N represents the amount of data.

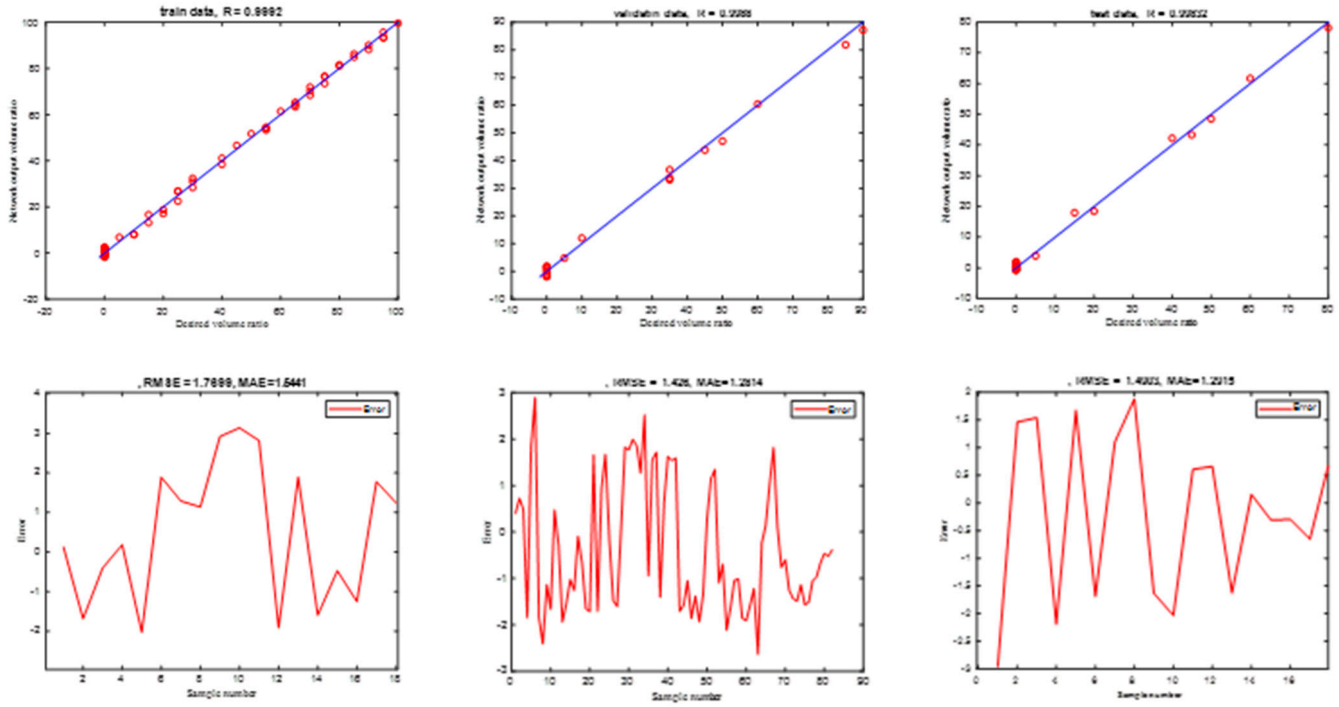

(**a**) (**b**) (**c**)

Figure 6. Performance of the designed neural network to determine the volumetric ratio of ethylene glycol: (**a**) training data, (**b**) validation data, and (**c**) test data.

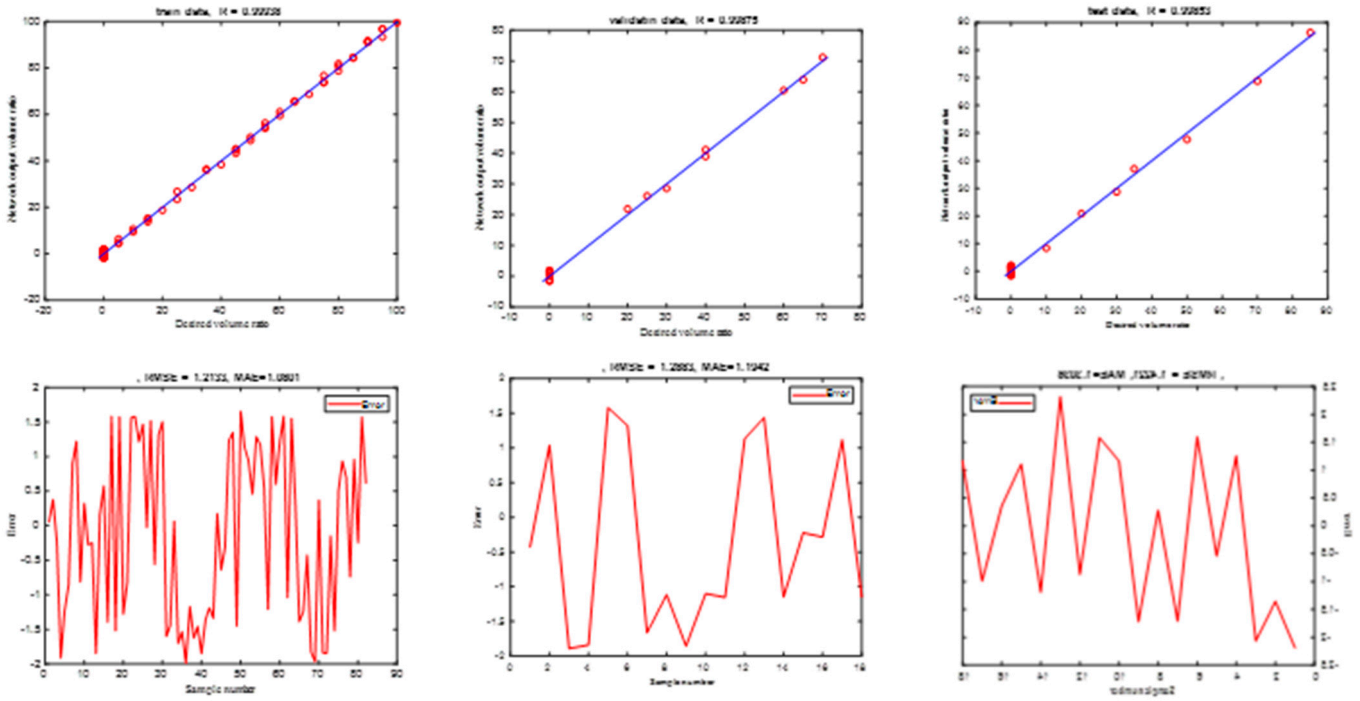

(**a**) (**b**) (**c**)

Figure 7. Performance of the designed neural network to determine the volumetric ratio of crude oil: (**a**) training data, (**b**) validation data, and (**c**) test data.

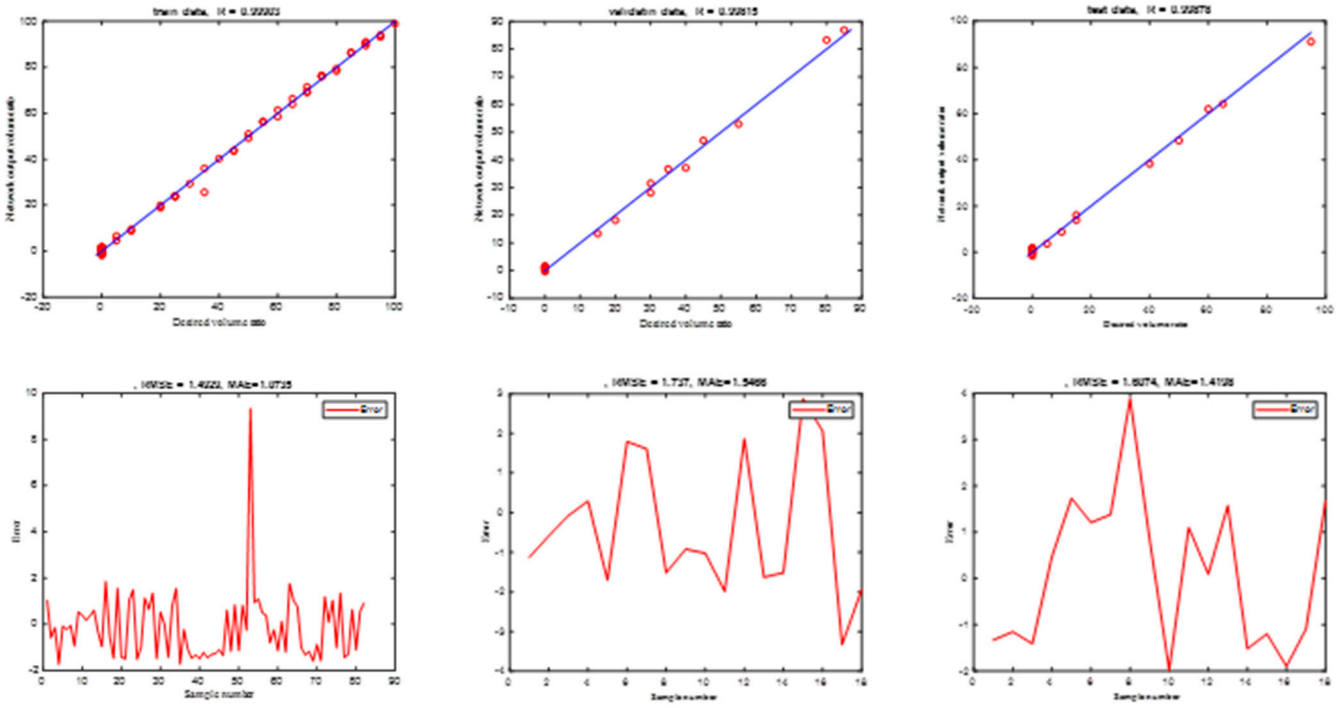

(**a**) (**b**) (**c**)

Figure 8. Performance of the designed neural network to determine the volumetric ratio of gasoil: (**a**) training data, (**b**) validation data, and (**c**) test data.

Table 2 shows the calculated errors for each of the predictor networks. The general process of determining the volume ratios of each oil product is shown in Figure 9.

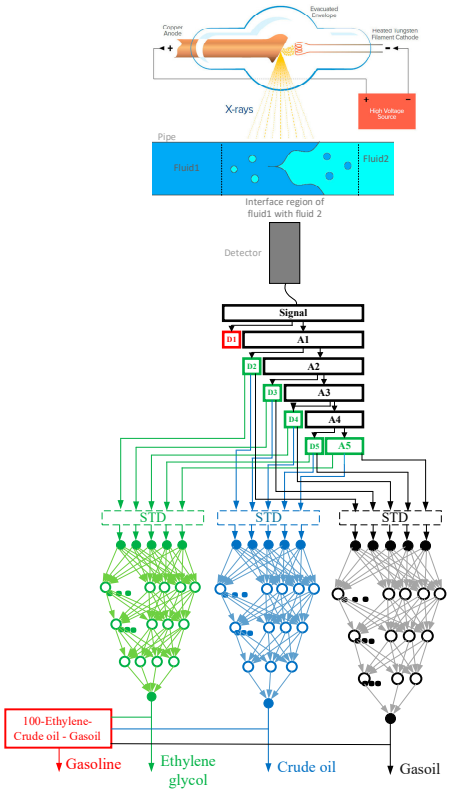

Figure 9. The general process of determining the volume ratio of each oil product.

Table 2. Calculated error for the implemented networks.

	Training Data		Validation Data		Test Data	
	RMSE	**MAE**	**RMSE**	**MAE**	**RMSE**	**MAE**
Ethylene glycol	1.42	1.28	1.76	1.54	1.49	1.29
Crude oil	1.21	1.08	1.28	1.19	1.42	1.30
Gasoil	1.49	1.07	1.73	1.54	1.60	1.41

6. Conclusions

In this study, the monitoring system included an X-ray tube and one NaI detector, simulated using the MCNPX transport code. After simulating the mixture of four petroleum products in different volume ratios and collecting data recorded by the detector, the DWT technique was used to extract the data features. Then, the extracted features were used to implement three MLP neural networks. It should be noted that after obtaining the volume ratio of three products, the volume ratio of the fourth product could easily be calculated. The three implemented neural networks predicted the volume ratio of ethylene glycol, crude oil, and gasoil with RMSEs of less than 1.77, 1.43, and 1.74, respectively. Although the X-ray tube, as well as radioisotopes, have been used in previous studies, applying the DWT method for feature extraction to improve the precision of this system is the most significant novelty of the current study.

Author Contributions: Conceptualization, M.A.S., E.N., and O.T.; software, A.A.B., M.A.S., and O.T.; writing—review and editing, M.A.S., M.B., E.N., O.T., and A.A.B.; funding acquisition, A.A.B., M.B., and O.T. All authors have read and agreed to the published version of the manuscript.

Funding: The authors extend their appreciation to the Deputyship for Research & Innovation, Ministry of Education in Saudi Arabia for funding this research work through the project number IFPHI-325-135-2020 and King Abdulaziz University, DSR, Jeddah, Saudi Arabia.

Institutional Review Board Statement: Not applicable.

Informed Consent Statement: Not applicable.

Data Availability Statement: Data are not contained within the article.

Conflicts of Interest: The authors declare no conflict of interest.

References

1. Salgado, C.M.; Brandão, L.E.B.; Conti, C.C.; Salgado, W.L. Density prediction for petroleum and derivatives by gamma-ray attenuation and artificial neural networks. *Appl. Radiat. Isot.* **2016**, *116*, 143–149. [CrossRef] [PubMed]
2. Salgado, W.L.; Dam, R.S.; Barbosa, C.M.; da Silva, A.X.; Salgado, C.M. Monitoring system of oil by-products interface in pipelines using the gamma radiation attenuation. *Appl. Radiat. Isot.* **2020**, *160*, 109125. [CrossRef]
3. Åbro, E.; Johansen, G.A. Improved void fraction determination by means of multibeam gamma-ray attenuation measurements. *Flow Meas. Instrum.* **1999**, *10*, 99–108. [CrossRef]
4. Nazemi, E.; Feghhi, S.A.H.; Roshani, G.H.; Peyvandi, R.G.; Setayeshi, S. Precise void fraction measurement in two-phase flows independent of the flow regime using gamma-ray attenuation. *Nucl. Eng. Technol.* **2016**, *48*, 64–71. [CrossRef]
5. Roshani, G.H.; Nazemi, E.; Feghhi, S.A.H. Investigation of using 60Co source and one detector for determining the flow regime and void fraction in gas–liquid two-phase flows. *Flow Meas. Instrum.* **2016**, *50*, 73–79. [CrossRef]
6. Chunguo, J.; Qiuguo, B. Flow regime identification of gas/liquid two-phase flow in vertical pipe using RBF neural networks. In Proceedings of the 2009 Chinese Control and Decision Conference, Guilin, China, 17–19 June 2009; IEEE: Piscataway, NJ, USA, 2009; pp. 5143–5147.
7. Peyvandi, R.G.; Rad, S.I. Application of artificial neural networks for the prediction of volume fraction using spectra of gamma rays backscattered by three-phase flows. *Eur. Phys. J. Plus* **2017**, *132*, 1–8.
8. Roshani, G.H.; Nazemi, E.; Roshani, M.M. Intelligent recognition of gas-oil-water three-phase flow regime and determination of volume fraction using radial basis function. *Flow Meas. Instrum.* **2017**, *54*, 39–45. [CrossRef]
9. Roshani, G.H.; Nazemi, E.; Roshani, M.M. Identification of flow regime and estimation of volume fraction independent of liquid phase density in gas-liquid two-phase flow. *Prog. Nucl. Energy* **2017**, *98*, 29–37. [CrossRef]

10. Roshani, G.H.; Nazemi, E.; Feghhi, S.A.H.; Setayeshi, S. Flow regime identification and void fraction prediction in two-phase flows based on gamma ray attenuation. *Measurement* **2015**, *62*, 25–32. [CrossRef]
11. Nazemi, E.; Roshani, G.H.; Feghhi, S.A.H.; Setayeshi, S.; Zadeh, E.E.; Fatehi, A. Optimization of a method for identifying the flow regime and measuring void fraction in a broad beam gamma-ray attenuation technique. *Int. J. Hydrog. Energy* **2016**, *41*, 7438–7444. [CrossRef]
12. Roshani, M.; Phan, G.T.; Ali, P.J.M.; Roshani, G.H.; Hanus, R.; Duong, T.; Corniani, E.; Nazemi, E.; Kalmoun, E.M. Evalu-ation of flow pattern recognition and void fraction measurement in two phase flow independent of oil pipeline's scale layer thickness. *Alex. Eng. J.* **2021**, *60*, 1955–1966. [CrossRef]
13. Roshani, M.; Phan, G.; Faraj, R.H.; Phan, N.-H.; Roshani, G.H.; Nazemi, B.; Corniani, E.; Nazemi, E. Proposing a gamma ra-diation based intelligent system for simultaneous analyzing and detecting type and amount of petroleum by-products. *Nucl. Eng. Technol.* **2021**, *53*, 1277–1283. [CrossRef]
14. Karami, A.; Roshani, G.H.; Khazaei, A.; Nazemi, E.; Fallahi, M. Investigation of different sources in order to optimize the nuclear metering system of gas–oil–water annular flows. *Neural Comput. Appl.* **2020**, *32*, 3619–3631. [CrossRef]
15. Roshani, M.; Sattari, M.A.; Ali, P.J.M.; Roshani, G.H.; Nazemi, B.; Corniani, E.; Nazemi, E. Application of GMDH neural network technique to improve measuring precision of a simplified photon attenuation based two-phase flowmeter. *Flow Meas. Instrum.* **2020**, *75*, 101804. [CrossRef]
16. Hanus, R.; Zych, M.; Petryka, L.; Jaszczur, M.; Hanus, P. Signals features extraction in liquid-gas flow measurements using gamma densitometry. Part 1: Time domain. In *EPJ Web of Conferences*; EDP Sciences: Les Ulis, France, 2016; Volume 114, p. 02035. [CrossRef]
17. Sattari, M.A.; Roshani, G.H.; Hanus, R.; Nazemi, E. Applicability of time-domain feature extraction methods and artificial intelligence in two-phase flow meters based on gamma-ray absorption technique. *Measurement* **2021**, *168*, 108474. [CrossRef]
18. Hanus, R.; Zych, M.; Petryka, L.; Jaszczur, M.; Hanus, P. Signals features extraction in liquid-gas flow measurements using gamma densitometry. Part 2: Frequency domain. In *EPJ Web of Conferences*; EDP Sciences: Les Ulis, France, 2016; Volume 114, p. 02036. [CrossRef]
19. Hosseini, S.; Roshani, G.H.; Setayeshi, S. Precise gamma based two-phase flow meter using frequency feature extraction and only one detector. *Flow Meas. Instrum.* **2020**, *72*, 101693. [CrossRef]
20. Sattari, M.A.; Roshani, G.H.; Hanus, R. Improving the structure of two-phase flow meter using feature extraction and GMDH neural network. *Radiat. Phys. Chem.* **2020**, *171*, 108725. [CrossRef]
21. Basahel, A.; Sattari, M.A.; Taylan, O.; Nazemi, E. Application of Feature Extraction and Artificial Intelligence Techniques for Increasing the Accuracy of X-ray Radiation Based Two Phase Flow Meter. *Mathematics* **2021**, *9*, 1227. [CrossRef]
22. Roshani, G.; Nazemi, E. Intelligent densitometry of petroleum products in stratified regime of two phase flows using gamma ray and neural network. *Flow Meas. Instrum.* **2017**, *58*, 6–11. [CrossRef]
23. Alamoudi, M.; Sattari, M.A.; Balubaid, M.; Eftekhari-Zadeh, E.; Nazemi, E.; Taylan, O.; Kalmoun, E.M. Application of Gamma Attenuation Technique and Artificial Intelligence to Detect Scale Thickness in Pipelines in Which Two-Phase Flows with Different Flow Regimes and Void Fractions Exist. *Symmetry* **2021**, *13*, 1198. [CrossRef]
24. Roshani, G.H.; Ali, P.J.M.; Mohammed, S.; Hanus, R.; Abdulkareem, L.; Alanezi, A.A.; Nazemi, E.; Eftekhari-Zadeh, E.; Kalmoun, E.M. Feasibility Study of Using X-ray Tube and GMDH for Measuring Volume Fractions of Annular and Stratified Regimes in Three-Phase Flows. *Symmetry* **2021**, *13*, 613. [CrossRef]
25. Roshani, M.; Phan, G.; Roshani, G.H.; Hanus, R.; Nazemi, B.; Corniani, E.; Nazemi, E. Combination of X-ray tube and GMDH neural network as a nondestructive and potential technique for measuring characteristics of gas-oil–water three phase flows. *Measurement* **2021**, *168*, 108427. [CrossRef]
26. Hosseini, S.; Taylan, O.; Abusurrah, M.; Akilan, T.; Nazemi, E.; Eftekhari-Zadeh, E.; Bano, F.; Roshani, G.H. Application of Wavelet Feature Extraction and Artificial Neural Networks for Improving the Performance of Gas–Liquid Two-Phase Flow Meters Used in Oil and Petrochemical Industries. *Polymers* **2021**, *13*, 3647. [CrossRef] [PubMed]
27. Hanus, R.; Zych, M.; Wilk, B.; Jaszczur, M.; Świsulski, D. Signals features extraction in radioisotope liquid-gas flow measurements using wavelet analysis. In *EPJ Web of Conferences*; EDP Sciences: Les Ulis, France, 2019; Volume 213, p. 02023.
28. Yu, G.; Gu, J.; Hou, L.; Li, Z.; Wang, Y.; Zhang, Y. Application of wavelet transform in γ-ray spectra analysis. *Sci. China Phys. Mech. Astron.* **2013**, *56*, 1735–1739. [CrossRef]
29. Zych, M.; Hanus, R.; Wilk, B.; Petryka, L.; Świsulski, D. Comparison of noise reduction methods in radiometric correlation measurements of two-phase liquid-gas flows. *Measurement* **2018**, *129*, 288–295. [CrossRef]
30. Brown, F.B.; Barrett, R.F.; Booth, T.E.; Bull, J.S.; Cox, L.J.; Forster, R.A.; Goorley, T.J.; Mosteller, R.D.; Post, S.E.; Prael, R.E.; et al. MCNP™ version 5. *Nucl. Instrum. Methods Phys. Res. Sect. B Beam Interact. Mater. At.* **2004**, *213*, 82–86.
31. Roshani, G.H.; Feghhi, S.A.H.; Mahmoudi-Aznaveh, A.; Nazemi, E.; Adineh-Vand, A. Precise volume fraction prediction in oil–water–gas multiphase flows by means of gamma-ray attenuation and artificial neural networks using one detector. *Measurement* **2014**, *51*, 34–41. [CrossRef]
32. Roshani, G.H.; Nazemi, E.; Roshani, M.M. Flow regime independent volume fraction estimation in three-phase flows using dual-energy broad beam technique and artificial neural network. *Neural Comput. Appl.* **2016**, *28*, 1265–1274. [CrossRef]
33. Hernandez, A.M.; Boone, J.M. Tungsten anode spectral model using interpolating cubic splines: Unfiltered X-ray spectra from 20 kV to 640 kV. *Med. Phys.* **2014**, *41*, 042101. [CrossRef] [PubMed]

34. Übeylı, E.D.; Güler, İ. Feature extraction from Doppler ultrasound signals for automated diagnostic systems. *Comput. Biol. Med.* **2005**, *35*, 735–764. [CrossRef]
35. Daubechies, I. The wavelet transform, time-frequency localization and signal analysis. *IEEE Trans. Inform. Theory* **1990**, *36*, 961–1005. [CrossRef]
36. Soltani, S. On the use of the wavelet decomposition for time series prediction. *Neurocomputing* **2002**, *48*, 267–277. [CrossRef]
37. Khounani, Z.; Hosseinzadeh-Bandbafha, H.; Nazemi, F.; Shaeifi, M.; Karimi, K.; Tabatabaei, M.; Aghbashlo, M.; Lam, S.S. Exergy analysis of a whole-crop safflower biorefinery: A step towards reducing agricultural wastes in a sustainable manner. *J. Environ. Manag.* **2021**, *279*, 111822. [CrossRef]
38. Sattari, M.T.; Avram, A.; Apaydin, H.; Matei, O. Soil Temperature Estimation with Meteorological Parameters by Using Tree-Based Hybrid Data Mining Models. *Mathematics* **2020**, *8*, 1407. [CrossRef]
39. Hosseinzadeh-Bandbafha, H.; Nazemi, F.; Khounani, Z.; Ghanavati, H.; Shafiei, M.; Karimi, K.; Lam, S.S.; Aghbashlo, M.; Tabatabaei, M. Safflower-based biorefinery producing a broad spectrum of biofuels and biochemicals: A life cycle assessment perspective. *Sci. Total Environ.* **2022**, *802*, 149842. [CrossRef] [PubMed]
40. Roshani, G.H.; Roshani, S.; Nazemi, E.; Roshani, S. Online measuring density of oil products in annular regime of gas-liquid two phase flows. *Measurement* **2018**, *129*, 296–301. [CrossRef]
41. Nazemi, F.; Karimi, K.; Denayer, J.F.; Shafiei, M. Techno-economic aspects of different process approaches based on brown macroalgae feedstock: A step toward commercialization of seaweed-based biorefineries. *Algal Res.* **2021**, *58*, 102366. [CrossRef]
42. Razzaq, A.; Wang, Y.; Chupradit, S.; Suksatan, W.; Shahzad, F. Asymmetric inter-linkages between green technology innovation and consumption-based carbon emissions in BRICS countries using quantile-on-quantile framework. *Technol. Soc.* **2021**, *66*, 101656. [CrossRef]
43. Charchi, N.; Li, Y.; Huber, M.; Kwizera, E.A.; Huang, X.; Argyropoulos, C.; Hoang, T. Small mode volume plasmonic film-coupled nanostar resonators. *Nanoscale Adv.* **2020**, *2*, 2397–2403. [CrossRef] [PubMed]
44. Nazemi, E.; Feghhi, S.; Roshani, G.; Setayeshi, S.A.; Peyvandi, R.G. A radiation-based hydrocarbon two-phase flow meter for estimating of phase fraction independent of liquid phase density in stratified regime. *Flow Meas. Instrum.* **2015**, *46*, 25–32. [CrossRef]
45. Roshani, S.; Roshani, S. Design of a high efficiency class-F power amplifier with large signal and small signal measure-ments. *Measurement* **2020**, *149*, 106991. [CrossRef]
46. Pourbemany, J.; Mirjalily, G.; Abouei, J.; Raouf, A.H.F. Load Balanced Ad-Hoc On-Demand Routing Basedon Weighted Mean Queue Length Metric. In Proceedings of the Electrical Engineering (ICEE), Iranian Conference on IEEE, Mashhad, Iran, 8–10 May 2018; pp. 470–475.
47. Lalbakhsh, A.; Afzal, M.U.; Esselle, K.P.; Manda, K. All-Metal Wideband Frequency-Selective Surface Bandpass Filter for TE and TM polarizations. *IEEE Trans. Antennas Propag.* **2022**, in press.
48. Pirasteh, A.; Roshani, S.; Roshani, S. A modified class-F power amplifier with miniaturized harmonic control circuit. *AEU Int. J. Electron. Commun.* **2018**, *97*, 202–209. [CrossRef]
49. Lalbakhsh, A.; Afzal, M.U.; Hayat, T.; Esselle, K.P.; Manda, K. All-metal wideband metasurface for near-field transformation of medium-to-high gain electromagnetic sources. *Sci. Rep.* **2021**, *11*, 9421. [CrossRef] [PubMed]
50. Jamshidi, M.B.; Roshani, S.; Talla, J.; Roshani, S.; Peroutka, Z. Size reduction and performance improvement of a microstrip Wilkinson power divider using a hybrid design technique. *Sci. Rep.* **2021**, *11*, 7773. [CrossRef] [PubMed]
51. Lalbakhsh, A.; Alizadeh, S.M.; Ghaderi, A.; Golestanifar, A.; Mohamadzade, B.; Jamshidi, M.B.; Mandal, K.; Mohyuddin, W. A Design of a Dual-Band Bandpass Filter Based on Modal Analysis for Modern Communication Systems. *Electronics* **2020**, *9*, 1770. [CrossRef]
52. Jamshidi, M.B.; Siahkamari, H.; Roshani, S.; Roshani, S. A compact Gysel power divider design using U-shaped and T-shaped reso-nators with harmonics suppression. *Electromagnetics* **2019**, *39*, 491–504. [CrossRef]
53. Roshani, S.; Roshani, S.; Zarinitabar, A. A modified Wilkinson power divider with ultra harmonic suppression using open stubs and lowpass filters. *Analog. Integr. Circuits Signal Process.* **2019**, *98*, 395–399. [CrossRef]
54. Lalbakhsh, A.; Mohamadpour, G.; Roshani, S.; Ami, M.; Roshani, S.; Sayem, A.S.M.; Alibakhshikenari, M.; Koziel, S. Design of a compact planar transmission line for miniaturized rat-race coupler with harmonics suppression. *IEEE Access* **2021**, *9*, 129207–129217. [CrossRef]
55. Roshani, S.; Roshani, S. Design of a very compact and sharp bandpass diplexer with bended lines for GSM and LTE applica-tions. AEU. *Int. J. Electron. Commun.* **2019**, *99*, 354–360. [CrossRef]
56. Lalbakhsh, A.; Jamshidi, M.B.; Siahkamari, H.; Ghaderi, A.; Golestanifar, A.; Linhart, R.; Talla, J.; Simorangkir, R.B.; Mandal, K. A Compact Lowpass Filter for Satellite Communication Systems Based on Transfer Function Analysis. *AEU-Int. J. Electron. Commun.* **2020**, *124*, 153318. [CrossRef]
57. Roshani, S.; Roshani, S. A compact coupler design using meandered line compact microstrip resonant cell (MLCMRC) and bended lines. *Wirel. Netw.* **2021**, *27*, 677–684. [CrossRef]
58. Pirasteh, A.; Roshani, S.; Roshani, S. Compact microstrip lowpass filter with ultrasharp response using a square-loaded mod-ified T-shaped resonator. *Turk. J. Electr. Eng. Comput. Sci.* **2018**, *26*, 1736–1746. [CrossRef]
59. Nouriani, A.; McGovern, R.A.; Rajamani, R. Step Length Estimation Using Inertial Measurements Units. In Proceedings of the 2021 American Control Conference (ACC), New Orleans, LA, USA, 25–28 May 2021; IEEE: Piscataway, NJ, USA, 2021; pp. 666–671.

60. Johar, M.G.M.; Ab Yajid, M.S.; Khatibi, A. Data Mining Technology and its Applications for Sales Productivity Analysis. *Syst. Rev. Pharm.* **2020**, *11*, 626–632.
61. Ghanbari, B. A new model for investigating the transmission of infectious diseases in a prey-predator system using a non-singular fractional derivative. *Math. Methods Appl. Sci.* **2021**. [CrossRef]
62. Nabti, A.; Ghanbari, B. Global stability analysis of a fractional SVEIR epidemic model. *Math. Methods Appl. Sci.* **2021**, *44*, 8577–8597. [CrossRef]
63. Alkabaa, A.S.; Nazemi, E.; Taylan, O.; Kalmoun, E.M. Application of Artificial Intelligence and Gamma Attenuation Techniques for Predicting Gas–Oil–Water Volume Fraction in Annular Regime of Three-Phase Flow Independent of Oil Pipeline's Scale Layer. *Mathematics* **2021**, *9*, 1460. [CrossRef]
64. Ghanbari, B. On the modeling of the interaction between tumor growth and the immune system using some new frac-tional and fractional-fractal operators. *Adv. Differ. Equ.* **2020**, *2020*, 585. [CrossRef]
65. Djilali, S.; Ghanbari, B. The influence of an infectious disease on a prey-predator model equipped with a fractional-order derivative. *Adv. Differ. Equ.* **2021**, *2021*, 20. [CrossRef]
66. Ghanbari, B. Chaotic behaviors of the prevalence of an infectious disease in a prey and predator system using fractional derivatives. *Math. Methods Appl. Sci.* **2021**, *44*, 9998–10013. [CrossRef]
67. Ghanbari, B. A fractional system of delay differential equation with nonsingular kernels in modeling hand-foot-mouth disease. *Adv. Differ. Equ.* **2020**, *2020*, 536. [CrossRef]
68. Ataii, F.; Khorasgani, S.M.S.; Abbasi, B.; Ghaffari, M. The Solution of Routing Problem of Vehicle with Capacity Aiming to Minimize Costs and Increase the Level of Satisfaction with the Use of Genetic Algorithms. *Fen Bilimleri Derg. (CFD)* **2015**, *36*. Available online: http://citeseerx.ist.psu.edu/viewdoc/download?doi:10.1.1.922.2811&rep=rep1&type=pdf (accessed on 19 October 2021).
69. Khorasgani, S.M.S.; Ghaffari, M. Developing a cellular manufacturing model considering the alternative routes, tool assignment, and machine reliability. *J. Ind. Eng. Int.* **2018**, *14*, 627–636. [CrossRef]
70. Moradi, M.J.; Hariri-Ardebili, M.A. Developing a Library of Shear Walls Database and the Neural Network Based Predictive Meta-Model. *Appl. Sci.* **2019**, *9*, 2562. [CrossRef]
71. Nazemi, B.; Rafiean, M. Forecasting house prices in Iran using GMDH. *Int. J. Hous. Mark. Anal.* **2021**, *14*, 555–568. [CrossRef]
72. Nazemi, B.; Rafiean, M. Modelling the affecting factors of housing price using GMDH-type artificial neural networks in Isfa-han city of Iran. *Int. J. Hous. Mark. Anal.* **2021**. [CrossRef]
73. Iyiola, K.; Rjoub, H. Using conflict management in improving owners and contractors relationship quality in the construction industry: The mediation role of trust. *SAGE Open* **2020**, *10*, 2158244019898834. [CrossRef]
74. Reyes-Campos, J.; Alor-Hernández, G.; Machorro-Cano, I.; Olmedo-Aguirre, J.O.; Sánchez-Cervantes, J.L.; Rodríguez-Mazahua, L. Discovery of Resident Behavior Patterns Using Machine Learning Techniques and IoT Paradigm. *Mathematics* **2021**, *9*, 219. [CrossRef]
75. de la Cruz, R.; Padilla, O.; Valle, M.A.; Ruz, G.A. Modeling Recidivism through Bayesian Regression Models and Deep Neural Networks. *Mathematics* **2021**, *9*, 639. [CrossRef]
76. Yoder Clark, A.; Blumenfeld, N.; Lal, E.; Darbari, S.; Northwood, S.; Wadpey, A. Using K-Means Cluster Analysis and Decision Trees to Highlight Significant Factors Leading to Homelessness. *Mathematics* **2021**, *9*, 2045. [CrossRef]
77. Zhuang, Y.; Yang, S.; Chupradit, S.; Nawaz, M.A.; Xiong, R.; Koksal, C. A nexus between macroeconomic dynamics and trade openness: Moderating role of institutional quality. *Bus. Process. Manag. J.* **2021**, *27*, 1703–1719. [CrossRef]
78. Alazzawi, F.J.I.; Shannaq, B. Machine learning Model for Generating Software Engineering Work Ethic's Course Syllabus Designed for Iraq's Work Environment. *Mach. Learn.* **2020**, *29*, 14794–14805.
79. Roshani, G.; Nazemi, E.; Roshani, M. Usage of two transmitted detectors with optimized orientation in order to three phase flow me-tering. *Measurement* **2017**, *100*, 122–130. [CrossRef]
80. Zych, M.; Petryka, L.; Kępiński, J.; Hanus, R.; Bujak, T.; Puskarczyk, E. Radioisotope investigations of compound two-phase flows in an open channel. *Flow Meas. Instrum.* **2014**, *35*, 11–15. [CrossRef]
81. Golijanek-Jędrzejczyk, A.; Mrowiec, A.; Hanus, R.; Zych, M.; Heronimczak, M.; Świsulski, D. The assessment of metrological properties of segmental orifice based on simulations and experiments. *Measurement* **2021**, *181*, 109601. [CrossRef]
82. Vlasák, P.; Chára, Z.; Matoušek, V.; Konfršt, J.; Kesely, M. Experimental investigation of fine-grained settling slurry flow behaviour in inclined pipe sections. *J. Hydrol. Hydromech.* **2019**, *67*, 113–120. [CrossRef]
83. Karami, A.; Roshani, G.H.; Nazemi, E.; Roshani, S. Enhancing the performance of a dual-energy gamma ray based three-phase flow meter with the help of grey wolf optimization algorithm. *Flow Meas. Instrum.* **2018**, *64*, 164–172. [CrossRef]
84. Golmohammadi, A.; Bani-Asadi, H.; Esmaeeli, H.; Hadian, H.; Bagheri, F. Facility layout for cellular manufacturing system under dynamic conditions. *Decis. Sci. Lett.* **2016**, *5*, 407–416. [CrossRef]
85. Khalaj, O.; Jamshidi, M.; Saebnoori, E.; Mašek, B.; Štadler, C.; Svoboda, J. *Hybrid Machine Learning Techniques and Computational Mechanics: Estimating the Dynamic Behavior of Oxide Precipitation Hardened Steel*; IEEE: Piscataway, NJ, USA, 2021.
86. Nouriani, A.; Moradi, H. Smooth switching in power control of wind turbines using a combination strategy of hysteresis and modified middle regions. *Sustain. Energy Technol. Assess.* **2020**, *37*, 100585. [CrossRef]
87. Jafarian-Namin, S.; Goli, A.; Qolipour, M.; Mostafaeipour, A.; Golmohammadi, A.M. Forecasting the wind power generation using Box-Jenkins and hybrid artificial intelligence: A case study. *Int. J. Energy Sect. Manag.* **2019**, *13*, 1038–1062. [CrossRef]

88. Nouriani, A.; Moradi, H. Variable speed wind turbine power control: A comparison between multiple MPPT based methods. *Int. J. Dyn. Control.* **2021**, 1–14. [CrossRef]
89. Wu, H.; Zhang, F.; Zhang, Z. Fundamental spray characteristics of air-assisted injection system using aviation kerosene. *Fuel* **2021**, *286*, 119420. [CrossRef]
90. Bhaskaran, S.; Marappan, R.; Santhi, B. Design and Analysis of a Cluster-Based Intelligent Hybrid Recommendation System for E-Learning Applications. *Mathematics* **2021**, *9*, 197. [CrossRef]
91. Roshani, S.; Roshani, S. Two-Section Impedance Transformer Design and Modeling for Power Amplifier Applications. *Appl. Comput. Electromagn. Soc. J.* **2017**, *32*, 1042–1047.
92. Mahmudova, S. Exploration of Intellectual Software Systems and Development of Conceptual Model. *Rev. Comput. Eng. Res.* **2020**, *7*, 1–11. [CrossRef]
93. Alkawaz, M.H.; Veeran, M.T.; Bachok, R. Digital image forgery detection based on expectation maximization algorithm. In Proceedings of the 2020 16th IEEE International Colloquium on Signal Processing & Its Applications (CSPA), Langkawi, Malaysia, 28–29 February 2020; IEEE: Piscataway, NJ, USA, 2020; pp. 102–105.
94. Elfaki, A.O.; Abouabdalla, O.A.; Fong, S.L.; Johar, G.M.; AIK, K.L.T.; Bachok, R. Review and future directions of the automated validation in software product line engineering. *J. Theor. Appl. Inf. Technol.* **2012**, *42*, 75–93.
95. Jayawardena, C.D.W.; Ahmad, A.; Jaharadak, A.A. Synthesis of digital transformation beyond technology perspective: Digital strategy, leadership & culture. *J. Crit. Rev.* **2020**, *7*, 349–357.
96. Al-Sanjary, O.I.; Ahmed, A.A.; Jaharadak AA, B.; Ali, M.A.; Zangana, H.M. Detection clone an object movement using an optical flow approach. In Proceedings of the 2018 IEEE Symposium on Computer Applications & Industrial Electronics (ISCAIE), Penang, Malaysia, 28–29 April 2018; IEEE: Piscataway, NJ, USA, 2018; pp. 388–394.
97. Zajmi, L.; Ahmed, F.Y.; Jaharadak, A.A. Concepts, methods, and performances of particle swarm optimization, backpropagation, and neural networks. *Appl. Comput. Intell. Soft Comput.* **2018**, *2018*, 9547212. [CrossRef]
98. Alsunki, A.A.M.; Ali, M.A.; Jaharadak, A.A.; Tahir, N.M. Framework of Software Developers Engagement Antecedents and Productivity-A Review. In Proceedings of the 2020 16th IEEE International Colloquium on Signal Processing & Its Applications (CSPA), Langkawi, Malaysia, 28–29 February 2020; IEEE: Piscataway, NJ, USA, 2020; pp. 302–307.
99. Shafiei, A.; Jamshidi, M.B.; Khani, F.; Talla, J.; Peroutka, Z.; Gantassi, R.; Baz, M.; Cheikhrouhou, O.; Hamam, H. A Hybrid Technique Based on a Genetic Algorithm for Fuzzy Multiobjective Problems in 5G, Internet of Things, and Mobile Edge Computing. *Math. Probl. Eng.* **2021**, *2021*, 9194578. [CrossRef]
100. Walid, W.; Awais, M.; Ahmed, A.; Masera, G.; Martina, M. Real-time implementation of fast discriminative scale space tracking algorithm. *J. Real-Time Image Process.* **2021**, *18*, 2347–2360. [CrossRef]
101. Shiri, A. A Novel Implementation of CORDIC Algorithm Based on Dynamic Microrotation Generation. *Mapta J. Electr. Comput. Eng.* **2021**, *3*, 17–27.
102. Nouriani, A.; McGovern, R.A.; Rajamani, R. *Step Length Estimation with Wearable Sensors Using a Switched-Gain Nonlinear Observer*; Elsevier: Amsterdam, The Netherlands, 2021.
103. Jawad, A.J.A.M.; Al Azzawi, F.J.I.; Biswas, A.; Khan, S.; Zhou, Q.; Moshokoa, S.P.; Belic, M.R. Bright and singular optical solitons for Kaup–Newell equation with two fundamental integration norms. *Optik* **2019**, *182*, 594–597. [CrossRef]
104. Ghanbari, B.; Yusuf, A.; Inc, M.; Baleanu, D. The new exact solitary wave solutions and stability analysis for the (2+1)-dimensional Zakharov—Kuznetsov equation. *Adv. Differ. Equ.* **2019**, *2019*, 49. [CrossRef]
105. Roshani, G.; Hanus, R.; Khazaei, A.; Zych, M.; Nazemi, E.; Mosorov, V. Density and velocity determination for single-phase flow based on radiotracer technique and neural networks. *Flow Meas. Instrum.* **2018**, *61*, 9–14. [CrossRef]
106. Ghanbari, B. Abundant exact solutions to a generalized nonlinear Schrödinger equation with local fractional derivative. *Math. Methods Appl. Sci.* **2021**, *44*, 8759–8774. [CrossRef]
107. Ghanbari, B.; Nisar, K.S.; Aldhaifallah, M. Abundant solitary wave solutions to an extended nonlinear Schrödinger's equation with conformable derivative using an efficient integration method. *Adv. Differ. Equ.* **2020**, *2020*, 328. [CrossRef]
108. Srivastava, H.M.; Günerhan, H.; Ghanbari, B. Exact traveling wave solutions for resonance nonlinear Schrödinger equation with intermodal dispersions and the Kerr law nonlinearity. *Math. Methods Appl. Sci.* **2019**, *42*, 7210–7221. [CrossRef]
109. Nurgalieva, K.S.; Saychenko, L.A.; Riazi, M. Improving the efficiency of oil and gas wells complicated by the formation of asphalt-resin-paraffin deposits. *Energies* **2021**, *14*, 6673. [CrossRef]
110. Tikhomirova, E.A.; Sagirova, L.R.; Khaibullina, K.S. A review on methods of oil saturation modelling using IRAP RMS. In *IOP Conference Series: Earth and Environmental Science*; IOP Publishing: Bristol, UK, 2019; Volume 378. [CrossRef]
111. Movchan, I.; Yakovleva, A.; Movchan, A.; Shaygallyamova, Z. Early assessment of seismic hazard in terms of voronezh massif-moscow depression contact. *Min. Miner. Depos.* **2021**, *15*, 62–70. [CrossRef]
112. Khaibullina, K.S.; Sagirova, L.R.; Sandyga, M.S. Substantiation and selection of an inhibitor for preventing the formation of asphalt-resin-paraffin deposits. Substanciação e seleção de um inibidor para evitar a formação de depósitos de asfalto-resina-parafina. *Period. Tche Quim.* **2020**, *17*, 541–551.
113. Khaibullina, K.S.; Korobov, G.Y.; Lekomtsev, A.V. Development of an asphalt-resin-paraffin deposits inhibitor and substantiation of the technological parameters of its injection into the bottom-hole formation zone. Desenvolvimento de um inibidor de depósito de asfalto-resinaparafina e subscantiação dos parâmetros tecnológicos de sua injeção na zona de formação de furo inferior. *Period. Tche Quim.* **2020**, *17*, 769–781.

114. Khaibullina, K. Technology to remove asphaltene, resin and paraffin deposits in wells using organic solvents. In Proceedings of the SPE Annual Technical Conference and Exhibition, Dubai, United Arab Emirates, 26 September 2016. [CrossRef]
115. Syah, R.; Alizadeh, S.M.; Nurgalieva, K.S.; Guerrero, J.W.G.; Nasution, M.K.M.; Davarpanah, A.; Metwally, A.S.M. A laboratory approach to measure enhanced gas recovery from a tight gas reservoir during supercritical carbon dioxide injection. *Sustainability* **2021**, *13*, 11606. [CrossRef]
116. Cui, L.; Weng, S.; Kirikkaleli, D.; Bashir, M.A.; Rjoub, H.; Zhou, Y. Exploring the role of natural resources, natural gas and oil production for economic growth of China. *Resour. Policy* **2021**, *74*, 102429. [CrossRef]
117. Djilali, S.; Ghanbari, B. Dynamical behavior of two predators–one prey model with generalized functional response and time-fractional derivative. *Adv. Differ. Equ.* **2021**, *2021*, 235. [CrossRef]
118. Ghanbari, B. On novel nondifferentiable exact solutions to local fractional Gardner's equation using an effective technique. *Math. Methods Appl. Sci.* **2021**, *44*, 4673–4685. [CrossRef]
119. Wang, K.; Wang, H.; Li, S. Renewable quantile regression for streaming datasets. *Knowl.-Based Syst.* **2021**, *235*. [CrossRef]
120. Ghanbari, B. On approximate solutions for a fractional prey–predator model involving the Atangana–Baleanu deriva-tive. *Adv. Differ. Equ.* **2020**, *2020*, 679. [CrossRef]
121. Ghanbari, B.; Atangana, A. Some new edge detecting techniques based on fractional derivatives with non-local and non-singular kernels. *Adv. Differ. Equ.* **2020**, *2020*, 435. [CrossRef]
122. Wang, K.; Li, S. Robust distributed modal regression for massive data. *Comput. Stat. Data Anal.* **2021**, *160*, 107225. [CrossRef]
123. Ghanbari, B.; Inc, M.; Rada, L. Solitary Wave Solutions to the Tzitzéica Type Equations Obtained by a New Efficient Approach. *J. Appl. Anal. Comput.* **2019**, *9*, 568–589. [CrossRef]
124. Rahman, G.; Nisar, K.S.; Ghanbari, B.; Abdeljawad, T. On generalized fractional integral inequalities for the monotone weighted Chebyshev functionals. *Adv. Differ. Equ.* **2020**, *2020*, 368. [CrossRef]
125. Taylor, J.G. *Neural Networks and Their Applications*; John Wiley & Sons Ltd.: Brighton, UK, 1996.
126. Gallant, A.R.; White, H. On learning the derivatives of an unknown mapping with multilayer feedforward networks. *Neural Netw.* **1992**, *5*, 129–138. [CrossRef]